International Journal of Mass Spectrometry 443 (2019) 93–100

Contents lists available at ScienceDirect

International Journal of Mass Spectrometry

journal homepage: www.elsevier.com/locate/ijms

Solution thermochemistry of concanavalin A tetramer conformers measured by variable-temperature ESI-IMS-MS

Tarick J. El-Baba, David E. Clemmer*

Department of Chemistry, Indiana University, Bloomington, IN, 47401, USA

ARTICLE INFO

Article history:
Received 10 April 2019
Received in revised form
31 May 2019
Accepted 13 June 2019
Available online 15 June 2019

ABSTRACT

Variable-temperature nano-electrospray ionization coupled with ion mobility spectrometry-mass spectrometry is used to investigate the thermal denaturation of the tetrameric protein concanavalin A. As the solution temperature is increased, changes in mass spectra and collision cross section distributions provide evidence for discrete structural changes that occur at temperatures that are ~40 to 50° below the temperature required for tetramer dissociation. The subtle structural changes are associated with four distinct tetramer conformations with unique melting temperatures. Gibbs-Helmholtz analysis of the free energies determined with respect to the most abundant "native" state yields heat capacities of $\Delta C_p = 1.6 \pm 0.3$, -2.2 ± 0.4, and -2.9 ± 1.6 kJ·K^{-1}·mol^{-1}, and temperature dependent enthalpies and entropies for the three non-native conformations. Analysis of the thermochemistry indicates that the high-temperature products are entropically stable until the threshold for tetramer dissociation, and changes in heat capacity are consistent with increases in solvation of polar residues. Our findings suggest these high-temperature non-native states result from an increase in disorder at surface exposed regions. Such studies provide valuable insight towards the structural details of non-native states.

1. Introduction

The protein data bank (PDB) now contains more than 150,000 structures, making it a tremendous resource for efforts aimed at predicting [1,2] and designing proteins [3–7]. While in recent years the accuracy of computed structures has improved markedly, most predictions focus on native conformations – only a small fraction of available data describe non-native or partially-folded forms (e.g., intermediates or denatured states) [1,8–10]. Characterization of these conformations will provide a better understanding of why different structures are favored. And, non-native structures are key to understanding fundamental aspects of proteostasis, the molecular origins of aging, as well as the etiology of misfolding based diseases, such as Alzheimer's and Parkinson's [11–13]. Studies of non-native states are difficult because these species are often disfavored; thus, the abundances of non-native states are low and they are often transient in nature as they may reform the native state. Additionally, non-native structures are especially sensitive to changes in solvent composition, [14–17], pH, [18,19], heat, [20,21], and small molecule binding [22,23].

A number of research groups have developed variable temperature (vT) electrospray ionization (ESI) sources to allow mass spectrometry (MS) readouts of structural changes that are induced in solution upon heating [21–33]. We recently combined these methods with ion mobility spectrometry (IMS) and found that it is possible to follow structural transitions associated with denaturation in remarkable detail. Inclusion of IMS provides a means of separating different conformations that are trapped upon evaporative cooling of ESI droplets. Compact (folded structures) with smaller collision cross sections have higher mobilities than elongated (unfolded) conformations [34]. By incrementally heating the protein solution it is possible to follow the equilibrium distribution of structures that is produced upon thermally denaturing the native state.

In this work, we use vT-ESI-IMS-MS to study the thermal denaturation of homotetrameric concanavalin A (ConA) from *C. ensiformis* (Scheme 1). ConA is a lectin commonly used in affinity and enrichment chromatography. Monomers (MW ~26 kDa) consist almost entirely of β-sheet structures [35] and can bind one transition metal (typically Mn^{2+}), one Ca^{2+}, and one saccharide in the active site [36]. ConA dimerizes at acidic pH [37,38]; above pH ~6, the protonation states of key acidic and basic residues (e.g., His-

* Corresponding author.
E-mail address: clemmer@indiana.edu (D.E. Clemmer).

https://doi.org/10.1016/j.ijms.2019.06.004
1387-3806/

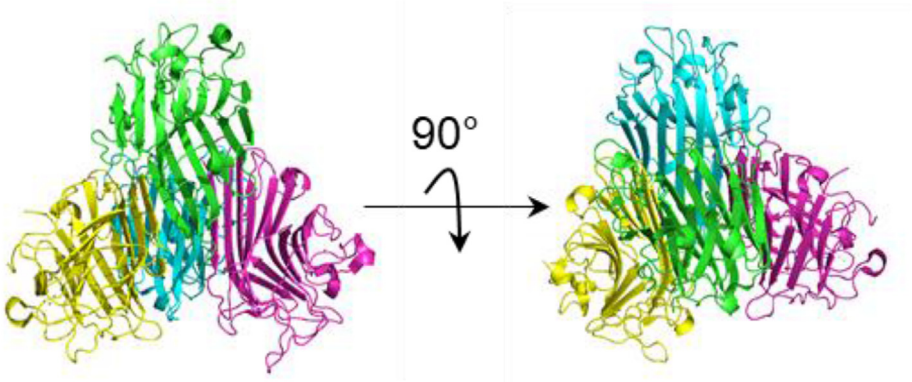

Scheme 1. Structure of concanavalin A shown in two different views (PDB: 5cna). The different colors delineate individual monomer units.

51 and His-127) promote the formation of the tetrameric form. Saccharide-bound tetramers have D_2 symmetry whereas ligand-free forms have equivalent interfaces between monomer units, arranging the dimers of dimers in a pseudo tetrahedron [39]. Differential scanning calorimetry studies indicate that tetrameric ConA is quite thermally stable and irreversibly dissociates at the melting temperature ($T_m \sim 350$ K) [40,41]. Below, we show that ligand-free tetramers undergo a subtle structural change prior to complex disassembly and tetramer dissociation. Analysis of IMS results provides evidence that the structural rearrangement involves four distinct species. We have developed and applied a model based on a Gibbs-Helmholtz analysis to capture insight to the enthalpy, entropy, and heat capacity changes for each state. We find that, prior dissociation, the thermochemistry for the products of melting are consistent with an enhancement in interactions of the complex with the bulk solvent – predissociative states that exist over a broad temperature range (~315 to ~345 K). Beyond this temperature, the signal for the tetramer disappears because the protein precipitates. We interpret the loss of signal as an irreversible dissociation event.

2. Experimental

2.1. General

All reagents were purchased from Sigma Aldrich (St. Louis, MO). All solvents were of the highest purity. ConA stock solutions were prepared at 100 μM in 150 mM ammonium acetate adjusted to pH ~ 6.9. Prior to analysis, solutions were desalted using Amicon 10K MWCO filters. Working solutions were prepared to 10 μM.

Electrospray capillaries (1.5 mm OD x 0.78 mm ID, filamented) were pulled to ~1-5 μm inner diameter using a Sutter Instruments P97 Flaming/Brown micropipette puller. ESI was initiated by applying a 0.8 – 1.1 kV potential to a platinum wire inserted into the analyte solution. A Waters Synapt G2 HDMS instrument was used for all IMS-MS experiments. The factory ESI source was removed and interlocks overridden. Our prototype vt-nESI source was coupled to the instrument to allow for temperature control of the analyte solution (see Supplementary Materials for more details). The heater and temperature control circuit were designed in house and based on our previous design [21]. Source conditions were optimized to minimize collisional activation [42,43]. Typical instrument parameters are as follows: source block temperature, 25°C; sampling cone, 30 – 35 V; extraction cone, 1 – 1.5 V; backing pressure, 5 – 10 mbar; trap gas pressure, ~5.0 x 10^{-2} mbar. Collision cross sections in N_2 buffer gas were estimated using the protocol developed by Ruotolo et al. using ubiquitin, transthyretin, and myoglobin as calibrants [44].

2.2. Data analysis

IMS-MS spectra were collected at different temperatures from 298 to 349 K (26 to 76 ℃); beyond this temperature, ConA irreversibly disassembles and forms insoluble aggregates [40]. All IMS-MS data were processed using UniDec [45] and TwimExtract [46] software packages. The peak centers and relative abundances for were determined by fitting a Gaussian function to each IMS peak at every temperature using the non-linear peak fitting tool in OriginPro (OriginLab, Northampton, MA). Relative abundances were used to compute equilibrium constants K_{eq}, which were referenced to conformer B,

$$K_j(T) = \frac{I_j(T)}{I_B(T)} \quad (1)$$

where $K_j(T)$ is the equilibrium constant of conformer j at temperature T, determined by dividing its intensity $I_j(T)$ at T by the intensity of B ($I_B(T)$). Temperature-dependent equilibrium constants were used to directly calculate the Gibbs free energy ΔG(T) using,

$$\Delta G(T) = -RT\ln(K_{eq}(T)) \quad (2)$$

where R is the gas constant. To account for changes in heat capacity, a Gibbs-Helmholtz analysis of ΔG vs temperature datasets was carried out. This was accomplished by a non-linear least-squares optimization of the values of ΔH_r and ΔS_r, the enthalpies and entropies determined at the reference temperature, T_r, (fixed at 298 K) and heat capacity (ΔC_p) using Equation (3), [47],

$$\Delta G(T) = \Delta H_r - T\Delta S_r + \Delta C_p\left[T - T_r - T\ln\left(\frac{T}{T_r}\right)\right] \quad (3)$$

Temperature-dependent enthalpies ΔH(T) and entropies ΔS(T) are calculated from equations (4) and (5), respectively.

$$\Delta H(T) = \Delta H_r + \Delta C_p(T - T_r) \quad (4)$$

$$\Delta S(T) = \Delta S_r + \Delta C_p\ln\left(\frac{T}{T_r}\right) \quad (5)$$

Equation (3) was coded into Python 3.6 and made use of numpy, [48], scipy, [49], and matplotlib [50] libraries. Uncertainties represent one standard deviation about the mean for three independent measurements. Theoretical collision cross sections were calculated from the crystal structure (PDB: 5cna) using IMPACT [51] by

averaging over 32 individual calculations.

3. Results and discussion

3.1. Analysis of structural change by MS charge state shifts

Fig. 1 shows mass spectra for ConA collected at T = 299, 319, and 339 K. Analysis of the mass spectrum collected at 299 K shows peaks between m/z = 4500 and 5500 which are signatures of the intact tetramer; a smaller charge state series can be found between m/z = 3200 − 3700 that are consistent with the mass of the dimeric form. Analysis of all mass spectra indicate that the narrow charge state envelope for the tetramer remains the dominant species across all temperatures sampled.

At low solution temperatures, the charge state envelope for the tetramers is centered about the 21+ ion. As the solution temperature is increased, the charge state distribution shifts to favor the 22+ species. The shift from low to high charge state is a signature of a structural change and is interpreted as a melting transition [24,25]. Interestingly, the dimer and monomer species do not substantially increase in abundance even at high temperatures, indicating the tetramer remains the most stable species in solution. While we do not observe tetramer dissociation, close inspection of solutions exposed to ~350 K for prolonged time shows evidence for precipitation, consistent with irreversible dissociation and aggregate formation.

A plot of the average charge state as a function of solution temperature shows that the shift from low to high charge state is gradual (Fig. 1, right panel). A fit of this sigmoidal transition yields a melting temperature $T_m = 316 \pm 2$ K. This is far below the expected melting temperature for ConA, which has been reported to be T_m ~ 353 K [40]. The subtle shift in charge with increasing temperature is evidence for a structural change that precedes tetramer dissociation. The mass spectrum recorded after cooling the T = 343 K solution is nearly identical to a mass spectrum collected for an unheated sample (see Supplementary Information). Because thermal dissociation of ConA leads to aggregation, the shift in charge must therefore be reporting on a reversible structural change involving the tetrameric form.

3.2. IMS analysis of structures involved in thermal denaturation

Insight about the structures involved in the melting transition can be gleaned by examining the IMS collision cross section distributions. Because only the solution temperature is varied, these spectra can be analyzed to obtain insight about the structural changes that occurred in solution as well as report on their relative abundances. Fig. 2 shows the collision cross section distributions for each charge state at three representative solution temperatures. Analysis of the low temperature collision cross section distribution for 19+ ions shows two peaks centered at 57.8 and 60.8 nm^2, respectively, which comprise <1% of the total ion population. The collision cross section distribution for the 20+ charge state, which contributes to ~10% of the total ion signal at low temperatures, is also comprised of two peaks – a small signal at $\Omega = 57.7$ nm^2 amid a major peak at $\Omega = 60.8$ nm^2. The dominant species present at low temperatures is the peak centered at $\Omega = 60.6$ nm^2 that populates the collision cross section distribution for the 21+ charge state. The 22+ species is also comprised of a single peak centered at $\Omega = 60.9$ nm^2 which makes up ~20% of the population at low temperatures. Finally, the collision cross section distributions for the low abundance 23+ charge state is made up of a sharp signal at $\Omega = 61.6$ nm^2 and a lower mobility shoulder at $\Omega = 64.2$ nm^2 – two peaks that are only formed in appreciable quantities at temperatures greater than ~ 320 K. Experimental collision cross sections for these ions are all near the calculated value $\Omega_{calc} = 60.8$ nm^2 from the atomic coordinates of the crystal structure, indicating that these signals are reporting on a distribution of structurally similar conformations.

As the solution temperature is increased, the populations of the peaks in the 19+ and 20+ collision cross section distributions decreases. These four signals respond with similar temperature dependencies, and as previously described, [21], we cannot rule out the possibility that IMS peaks with similar collision cross sections that also respond alike to changes in temperature arise from a common solution phase conformer. Therefore, we group these signals together and assign them as conformer A. Conformer B is made up of the single IMS peak in the 21+ charge state which also decreases in abundance as temperature is increased. The two species which emerge at elevated temperatures are conformer C (the single feature in 22+) and the low abundance signals in the collision cross section distributions are 23+ assigned as conformer D.

Fig. 3 shows a plot of the relative abundances at each temperature for these four conformations (i.e., melting curves). It is interesting to consider the loss of conformers A and B in more detail. Conformer A decreases from ~12% to ~5% of the total population from low to high temperatures and has a melting temperature of $T_m = 310 \pm 3$ K. Conformer B, which is the dominant species at low solution temperatures, decreases from ~70% to ~40% of the total population at high temperatures, and has $T_m = 318 \pm 2$ K.

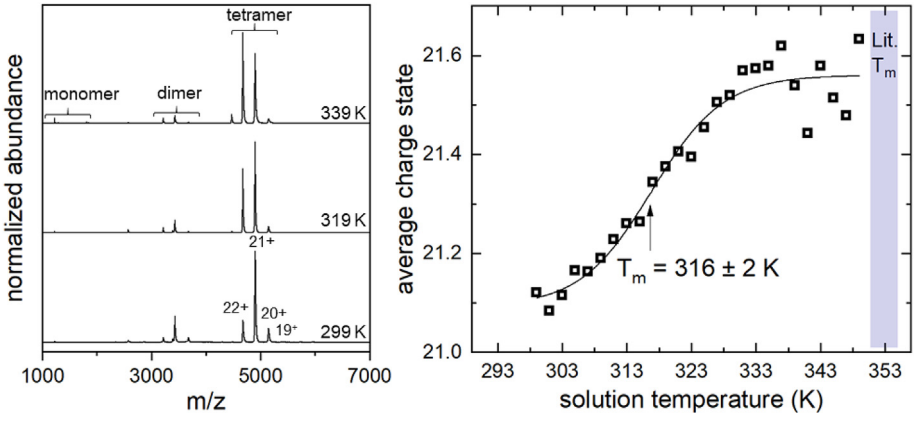

Fig. 1. (left) mass spectral data recorded at representative solution temperatures; (right) average charge state as a function of solution temperature. The melting temperature of 316 ± 2 K indicates a structural change prior to dissociation. Blue shaded region designates reported T_m values for tetramer dissociation.

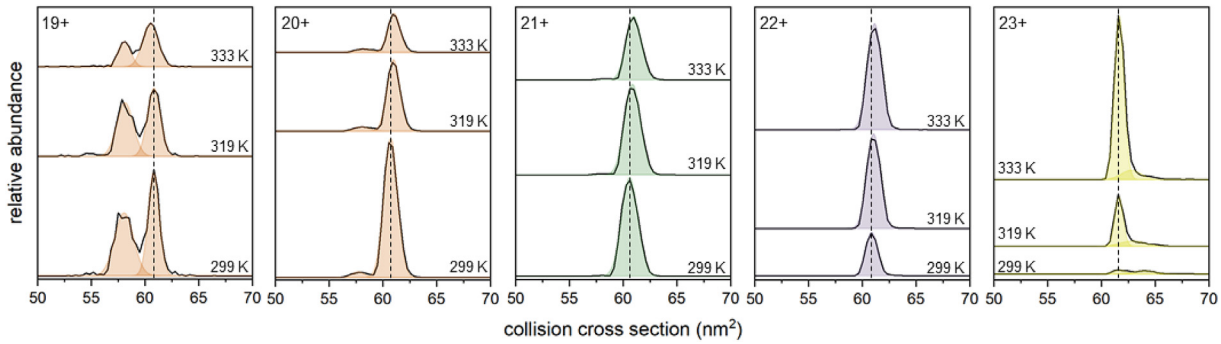

Fig. 2. Collision cross section distributions for each charge state of ConA. Shaded regions denote each conformer: A – peach, B – green, C – purple, D – yellow. Dotted lines indicate the position of the peak center at 299 K. (For interpretation of the references to color in this figure legend, the reader is referred to the Web version of this article.)

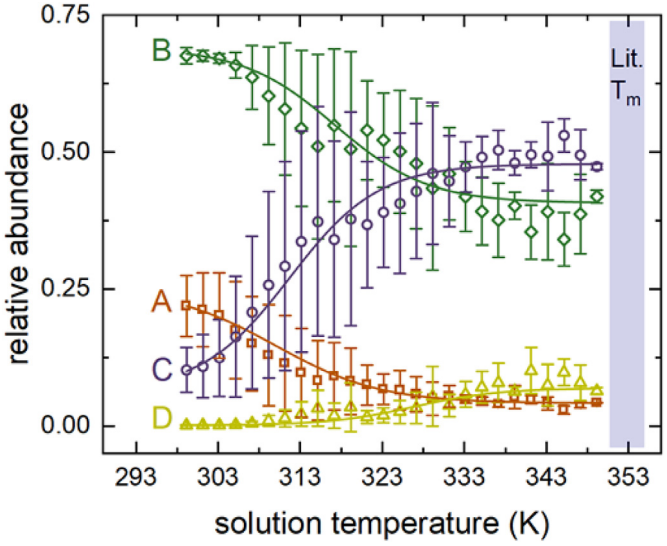

Fig. 3. Abundance profile for each conformer as a function of solution temperature. T_m values for each conformer are: A – 310 ± 3 K; B – 318 ± 2 K; C – 315 ± 2 K; D – 327 ± 2 K. Blue shaded region designates reported T_m values for tetramer dissociation. (For interpretation of the references to color in this figure legend, the reader is referred to the Web version of this article.)

These mobility-derived melting curves have T_m values that are nearly 40 K lower than the value measured for the ensemble average determined from calorimetry measurements [40,41]. This requires that two structurally similar species undergo distinct structural rearrangements far below the temperature required to dissociate the complex – else their melting curves would be identical.

This analysis can be extended to the products of melting. Conformer C, which is the dominant product of melting, begins at ~13% of the total population at T = 299 K and increases to ~50% at T = 333 K with midpoint formation temperature $T_f = 315 \pm 1$ K. The low abundance conformer D emerges with increases in solution temperature and has $T_f = 327 \pm 2$ K. Differences in the temperature profiles and formation temperatures for these species provides further evidence for two distinct products of melting which retain enough stability to resist dissociation.

3.3. Thermal denaturation of ConA involves a gradual structural change

Fig. 4 shows that coupled to the changes in IMS peak population is a subtle shift in peak center. At low-solution temperatures, each dominant IMS peak is centered near 60 nm^2, indicating the conformers have closely related topologies. As the solution temperature increases, the peak centers within each collision cross section distribution shift (also delineated by the dashed lines in Fig. 2). For example, the peak centers for conformers B and C show a slight increase at elevated temperatures. As these are the major signals at every temperature, we anticipate they are reporting on the dominant solution-phase structures. Some conformers shift to lower collision cross sections with increases in temperature, as is observed for the feature at ~58.1 nm^2 in 19+ and the shoulder at ~64.0 nm^2 in the 23+ charge state. This may suggest the presence of several additional unique but low abundance conformations not captured by comparing temperature-dependent abundance profiles. However, these changes are linear with respect to temperature and therefore do not behave as typical cooperative melting transitions. We conservatively do not interpret these as discrete melting events, but instead consider the possibility that the changes may originate from differences in protonation state (i.e., protomers). Nonetheless we observe that on average, the abundant features in each collision cross section distribution shift to higher values. Fig. 4 illustrates this by plotting the weighted average collision cross section at each solution temperature, which has an excellent correlation with temperature and provides a clue that the structural rearrangement involves an extremely subtle change in topology.

In the absence of saccharides, tetrameric ConA has essentially equivalent monomers arranged in a pseudo-tetrahedron. Any structural change within a subunit must also occur symmetrically across entire complex. We consider two possibilities that may give rise to such a subtle structural change with a clear temperature dependence: (1) regions on the surface of each subunit lose some elements of structure, causing them to unfold, and/or (2) the entire complex expands isotropically due to weakened intermolecular forces between subunits. Whatever the underlying motion may be, the tetrameric form must remain intact. Both cases result in a gradual thermal expansion of the tetrameric complex. Since IMS measurements are unable to distinguish between such topological subtleties with absolute certainty, we cannot rule out either case. However, we would expect the latter case to result in exposure of several titratable amino acid side chains (e.g., His-51, His-127) that are expected to capture protons during the process of ESI [52]. These residues form key intramolecular interactions in the interface between subunits. Changes to the protonation states of these species will alter the hydrogen bonding patterns and increase the Coulomb repulsion between subunits. In this scenario, the intact tetramer would likely not survive the transfer to the gas-phase. Therefore, we consider the former case to be more likely.

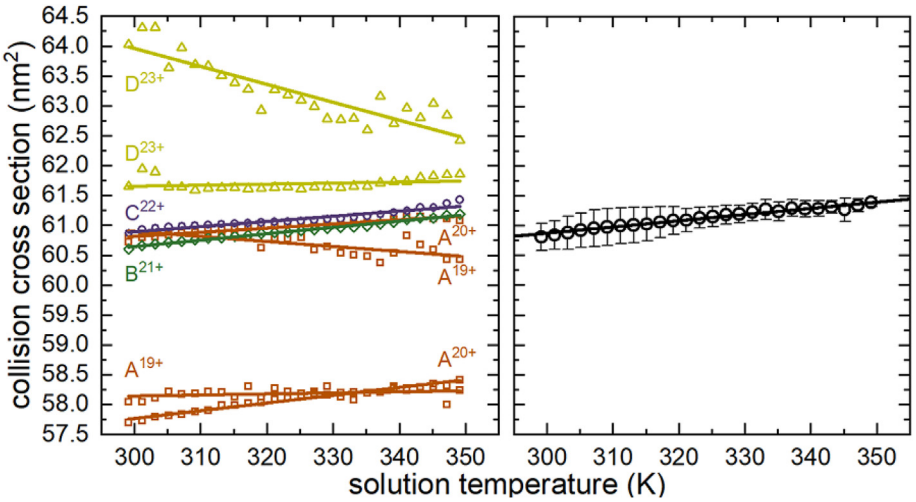

Fig. 4. Plots showing peak center as a function of solution temperature for each signal (left) and the weighted average (right) across each collision cross section distribution.

3.4. Capturing the thermodynamics mediating the structural rearrangement

The ability to monitor the abundances of both native and non-native conformations with such high fidelity provides the rare opportunity to capture their thermodynamic stabilities. Fig. 5A shows a plot of the calculated Gibbs free energy as a function of solution temperature for each conformer (using Eqs. (1) and (2)). The curvature of these plots is a signature of a heat capacity change. Therefore, we fit these data to the non-linear form of the Gibbs-Helmholtz equation [47] (Eq. (3)) to determine the enthalpy and entropy at 298 K and associated change in ΔC_p. The solid lines in Fig. 5A show the model has excellent agreement with data; the derived values for ΔH, ΔS, and ΔC_p (at 298 K) are listed in Table 1 and plotted in Fig. 5B.

Fersht, [53], Privalov, [54], Sharp, [55], and Sturtevant [56] have argued that these thermochemical values provide insight about some molecular details involved with thermal denaturation. Folded structures are stabilized by intramolecular contacts (e.g., salt-bridges, hydrogen bonds, sidechain packing). This stabilization (a decrease in enthalpy) occurs at the expense of configurational freedom (ΔS). As the temperature is increased, many of the stabilizing intramolecular bonding interactions (in the folded state) are lost; this allows the protein to adopt new conformations and the new structures that are formed are expected to have a greater configurational entropy and a less favorable enthalpy. From this, one expects that the native state will have a higher ΔC_p than the denatured forms. However, the thermodynamic contributions from the solvent must also be considered. As less ordered forms of the protein are favored at elevated temperatures, ordered water networks can assemble around exposed non-polar residues leading to an increase in ΔC_p of the denatured states. The formation of these "icebergs" maximizes the number of favorable hydrogen bonds formed between the solvent molecules, consequently restricting their accessible configurations. As temperature is increased, these hydrogen bonding networks also become unstable and the loss of these structures also contribute to an increase in ΔC_p in the denatured conformations. In contrast, interaction between water and exposed polar residues cause ΔC_p to be small or negative, and decreases the overall order of the solvent, resulting in a favorable ΔS component (more conformational freedom) at the expense of ΔH (i.e., arising from fewer hydrogen bonding interactions). The effects of polar and non-polar solvation are additive and is the major contribution to heat capacity differences between the native and

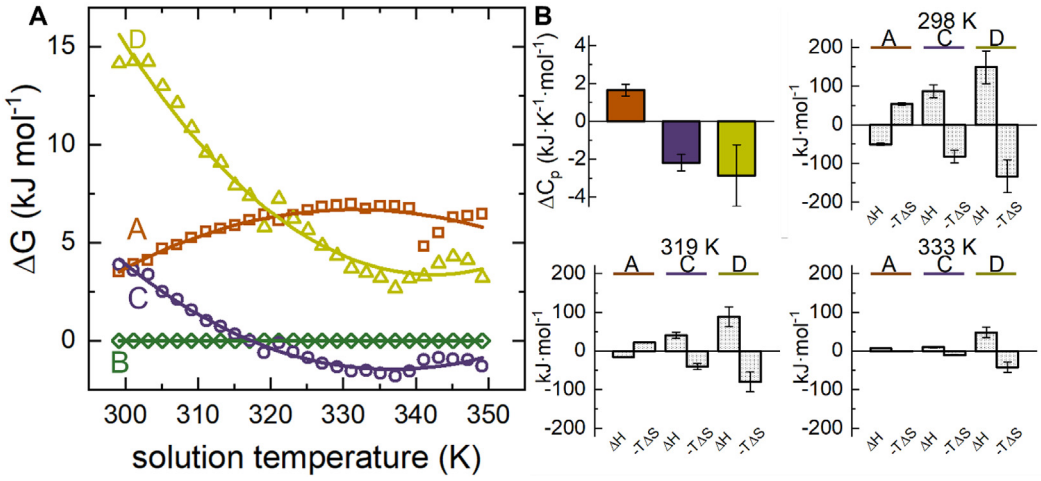

Fig. 5. (A) Gibbs-Helmholtz plot of calculated ΔG as a function of solution temperature and (B) heat capacities and thermodynamic values at 298 K, 319 K, and 333 K ΔG values determined with respect to conformer B.

Table 1
Thermochemistry of conformers A, C, and D at 298 K.[a]

Conformer	ΔH (kJ·mol^{-1})	ΔS (J·K^{-1}mol^{-1})	$-T\Delta S$ (kJ·mol^{-1})	ΔC_p (kJ·K^{-1}·mol^{-1})
A	-50.4 ± 3.1	-179.8 ± 9.5	53.6 ± 2.8	1.6 ± 0.3
C	86.6 ± 17.0	275.1± 54.7	-82.0 ± 16.3	-2.2 ± 0.4
D	148.6 ± 42.6	446.3 ± 141.5	-133.0 ± 42.2	-2.9 ± 1.6

[a] Values are for a 150 mM ammonium acetate solution at pH 6.9.

"denatured" forms. Because the hydrophobic effect is the driving force behind folding, heat-denatured forms are expected to have an enhancement in non-polar solvation as these residues emerge from buried regions in the folded polypeptide, i.e., the overall ΔC_p is positive [53].

Analysis of the ΔC_p values in Fig. 5B shows that the magnitudes are small, suggesting that the conformers share a common structural motif. The positive ΔC_p for conformer A is a signature of non-polar amino acid solvation, whereas the negative ΔC_p values for conformers C and D are indicative of solvation of hydrophilic residues by water. The negative ΔC_p values for the product conformers was unexpected, as high-temperature unfolded states typically have more hydrophobic residues exposed to the surrounding solvent as compared to compact, folded forms. Deviation from this expected trend suggests the product conformers adopt flexible structures that contribute to an overall decrease in solvent-protein order.

The ΔC_p terms cause the ΔH and ΔS to have a significant temperature dependence. Also shown in Fig. 5B are the enthalpies and entropies at three representative temperatures calculated from Eq. (2) and Eq. (3). At 298 K, conformer A is the most energetically favorable species at the expense of an unfavorable entropic component. Conformers C and D are both formed unfavorably with respect to enthalpy and are instead stabilized by the increase in entropy. As temperature is increased, the enthalpic component for conformer A is driven to values that are increasingly more positive (i.e., unfavorable). By 333 K, the entropy becomes stabilizing amid an unfavorable enthalpic component; the abundance of this species decreases at increased temperatures, likely because the increase in entropy is not enough to compensate the destabilizing enthalpic component. Conformers C and D are stable at high temperatures. At 319 K, both are formed endothermically and are therefore stabilized by the entropic components. The 333 K thermochemistry shows the values for entropy have decreased but remains positive; these species are still formed endothermically.

Both high temperature products are entropically stabilized, have increased collision cross sections at high temperatures, and have negative ΔC_p values. These factors suggest that formation of conformers C and D provide an increase in the disorder of the system. Most importantly, amid this structural change, the tetramer is still stable in solution. Therefore, any conformational changes responsible for forming these high temperature species is anticipated to arise from an increase in disorder at the surface exposed regions rather than a loss of structure in the major fold or a breakdown in the subunit interfaces responsible for stabilizing the tetramer [35]. This would lead to an increase in the overall configurational entropy of the protein and enhance the solvent-protein interactions at regions that are already surface exposed. This would not significantly increase ΔC_p since these regions are already interacting with solvent. We anticipate that the increase in disorder at the surface exposed loops and turns would provide more opportunities for intermolecular solvent-conformation interactions and would allow the hydrogen bonding network present in the bulk to extend closer to the protein complex. While we cannot eliminate the possibility that the entire complex expands isotropically, this would likely create cavities between subunits that can be occupied by solvent (like in the active site) [36–39] which increases the order significantly.

3.5. Temperature-dependent enthalpies and entropies

Capturing changes in the heat capacity provides the rare opportunity to determine the temperature-dependent enthalpies and entropies in a conformationally-resolved fashion. Fig. 6 plots the enthalpies, entropies, and Gibbs free-energies for conformers A, C, and D calculated from Eq. (2) and (3), and [fx]. Visual inspection of the low temperature region shows that conformer A is the only favored form. Analysis of the enthalpic and entropic components indicate that conformer A maintains stability by enthalpy amid an unfavorable entropic component. As temperature is increased, the dashed and dotted lines coalesce, indicating that the entropic penalty is minimized at the expense of energy. Thus, while the system becomes more accessible at increased temperatures, fewer strong interactions are available. This is likely the reason that this species is not made in appreciable quantities at high temperatures. Interestingly, the enthalpic and entropic terms for conformers C and D are not only different, they show a sign inversion with respect to those found for conformer A. In other words, at low temperatures, these conformers are the enthalpically disfavored, but entropically preferred forms of ConA. Analysis of the magnitudes of the entropy and enthalpy values shows their summation will result in similar free energies (i.e., $\Delta G \pm 25$ kJ mol^{-1}) across the temperature range, in good agreement with the notion that folding and assembly result from a delicate balance of marginally-stabilizing interactions [53].

As the temperature is increased, the entropy and enthalpy values for each conformation converge towards zero but are still correlated such that their summation will always yield similar free

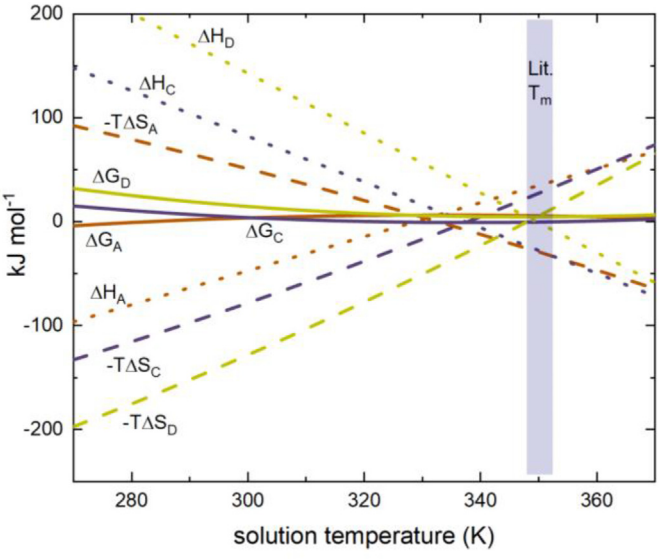

Fig. 6. Calculated thermodynamic values from 270 – 375 K.

energies. As an example, at T = 300 K, $\Delta H_C = 82.2 \pm 16.1$ kJ·mol^{-1} and, $-T\Delta S_C = -78.1 \pm 15.5$ kJ·mol^{-1}, resulting in a free energy of $\Delta G_C = 4.1 \pm 3.1$ kJ·mol^{-1}, and at T = 365 K, $\Delta H_C = -60.6 \pm 11.9$ kJ·mol^{-1} and $-T\Delta S_C = 62.2 \pm 12.4$ kJ·mol^{-1}, yielding $\Delta G_C = 1.6 \pm 0.5$ kJ·mol^{-1}. This trend is consistent across all temperatures sampled; convergence of the ΔH and -TΔS components such that only a narrow range of free energies is accessible is a signature of an increasingly rugged landscape, which facilitates the coexistence of several structures. Our calculations indicate that conformer A should be reestablished as the preferred state above T = 350 K. But, at this temperature, the system overcomes the barrier for tetramer dissociation creating a competing kinetic process that precludes our ability to probe equilibria.

4. Summary and conclusions

vT-ESI-IMS-MS was used to study tetrameric ConA. The temperature-dependent MS data provided a clue for a reversible structural change that precedes tetramer dissociation. Analysis of the abundances of peaks in each collision cross section distribution provided evidence for four unique conformations that have discrete T_m values far below the melting temperature of 350 K reported for tetramer dissociation [40,41]. Collision cross sections for all conformers were found to shift linearly with increasing temperature. We interpret this continuous change as evidence that the structural change corresponds to a uniform change throughout the complexes. The structural change is reversible, indicating the subtle rearrangement does not induce large changes to the overall topology. Plots of free energy versus temperature for each conformer were analyzed using the Gibbs-Helmholtz relation and temperature dependent thermochemistry was reported. Heat capacities for product states C and D were consistent with solvation of polar residues; the favorable entropic components suggest the structural change involves a loss of structure unfolding at solvent-exposed regions. Entropy stabilized these high-temperature forms up to the point of tetramer dissociation. While not directly observed, calculation of the thermochemistry at temperatures inaccessible to experiment (due to complex dissociation or aggregation) can be used to further understand the driving forces responsible for establishing structure.

The authors declare no competing financial interest.

Acknowledgements

This work was supported in part from funds from the National Institutes of Health (5R01GM121751-02, and 1R01GM131100-01) and the Waters Corporation. TJE gratefully acknowledge support from the Indiana University College of Arts and Sciences Dissertation Research Award.

Appendix A. Supplementary data

Supplementary data to this article can be found online at https://doi.org/10.1016/j.ijms.2019.06.004.

References

[1] K.A. Dill, J.L. MacCallum, The protein-folding problem, 50 years on, Science 338 (2012) 1042–1046.
[2] R.F. Service, Google's DeepMind aces protein folding, Science (2018), https://doi.org/10.1126/science.aaw2747.
[3] A.R. Buller, P. van Roye, J.K.B. Cahn, R.A. Scheele, M. Herger, F. Arnold, Directed evolution mimics allosteric activation by stepwise tuning of the conformational ensemble, J. Am. Chem. Soc. 140 (2018) 7256–7266.
[4] P.J. Almhjell, C.E. Boville, F.H. Arnold, Engineering enzymes for noncanonical amino acid synthesis, Chem. Soc. Rev. 47 (2018) 8980–8997.
[5] A. Chevalier, D.-A. Silva, G.J. Rocklin, D.R. Hicks, R. Vergara, P. Murapa, S.M. Bernard, L. Zhang, K.-H. Lam, B. Guorui, C.D. Bahl, S.-I. Miyashita, I. Goreshnik, J.T. Fuller, M.T. Koday, C.M. Jenkins, T. Colvin, L. Carter, A. Bohn, C.M. Bryan, A.D. Fernandez-Velasco, L. Stewart, M. Dong, X. Huang, R. Jin, I.A. Wilson, D.H. Fuller, D. Baker, Massively parrel de novo protein design for targeted therapeutics, Nature 550 (2017) 74–79.
[6] C. Zibo, s. E. Boyken, M. Jia, F. Busch, D. Flores-Solis, M.J. Bick, P. Lu, Z.L. VanAernum, A. Sahasrabuddhe, R.A. Langan, S. Bermeo, T.J. Brunette, V.K. Mulligan, L.P. Carter, F. DiMaio, N.G. Sgourakis, V.H. Wysocki, D. Baker, Programmable design of orthogonal protein heterodimers, Nature 565 (2019) 106–111.
[7] C.B. Anfinsen, Principles that govern the folding of protein chains, Science 181 (1973) 223–230.
[8] K.A. Dill, H.S. Chan, From Leventhal to pathways to funnels, Nat. Struct. Biol. 4 (1997) 10–19.
[9] A.R. Fersht, From the first protein structures to our current knowledge of protein folding: delights and skepticisms, Nat. Rev. Mol. Cell Biol. 9 (2008) 650–654.
[10] S.W. Englander, L. Mayne, The nature of protein folding pathways, Proc. Natl. Acad. Sci. U.S.A. 111 (2014) 15873–15880.
[11] R.J.W. Truscott, K.L. Schey, M.G. Friedrich, Old proteins in man: a field in its infancy, Trends Biochem. Sci. 41 (2016) 654–664.
[12] P. Leuenberger, s. Ganscha, A. Kahraman, V. Cappellitti, P.J. Boersema, C. von Mering, M. Claassen, P. Picotti, Cell-wide analysis of protein thermal unfolding reveals determinants of thermostability, Science 355 (2017) eaai7825.
[13] G.J. Rocklin, T.M. Chidyausiku, I. Goreshnik, A. Ford, S. Houliston, A. Lemak, L. Carter, R. Ravichandran, V.K. Mulligan, A. Chevalier, C.H. Arrowsmith, D. Baker, Global analysis of protein folding using massively parallel design, synthesis, and testing, Science (2017) 168–175.
[14] C.N. Pace, Determination and analysis of urea and guanidine hydrochloride denaturation curves, Methods Enzymol. 131 (1986) 266–280.
[15] H. Shi, D.E. Clemmer, Evidence for two new solution states of ubiquitin by IMS-MS analysis, J. Phys. Chem. B 118 (2014) 3498–3506.
[16] T.L. Religa, J.S. Markson, U. Mayor, S.M.V. Freund, A.R. Fersht, Solution structure of a protein denatured state and folding intermediate, Nature 437 (2005) 1053–1056.
[17] C.N. Pace, K.L. Shaw, Linear extrapolation method for analyzing solvent denaturation curves, Proteins 41 (2000) 1–7.
[18] D.E. Anderson, W.J. Becktel, F.W. Dahlquist, pH-induced denaturation of proteins: a single salt bridge contributes 3-5 kcal/mol to the free energy of folding of T4 lysozyme, Biochemistry 29 (1990) 2403–2408.
[19] L. Konermann, D.J. Douglas, Acid-induced unfolding of cytochrome c at different methanol concentrations: electrospray ionization mass spectrometry specifically monitors changes in the tertiary structure, Biochemistry 36 (1997) 12296–12302.
[20] S.E. Jackson, A.R. Fersht, Folding of chymotrypsin inhibitor 2. 1. Evidence for a two-state transition, Biochemistry 30 (1991) 10428–10435.
[21] T.J. El-Baba, D.W. Woodall, S.A. Raab, D.R. Fuller, A. Laganowsky, D.H. Russell, D.E. Clemmer, Melting proteins: evidence for multiple stable structures upon thermal denaturation of native ubiquitin from ion mobility spectrometry-mass spectrometry measurements, J. Am. Chem. Soc. 139 (2017) 6306–6309.
[22] J.D. Eschweiler, R.M. Martini, B.T. Ruotolo, Chemical probes and engineered constructs reveal a detailed unfolding mechanism for a solvent-free multi-domain protein, J. Am. Chem. Soc. 139 (2016) 534–540.
[23] D.S. Chorev, L.A. Baker, D. Wu, V. Beilsten-Edmands, S.L. Rouse, T. Zeev-Ben-Mordehai, C. Jiko, F. Samsudin, C. Gerle, S. Khalid, A.G. Stewart, S.J. Matthews, K. Gruenewald, C.V. Robinson, Protein assemblies ejected directly from native membranes yield complexes for mass spectrometry, Science 362 (2018) 829–834.
[24] U.A. Mirza, S.L. Cohen, B.T. Chait, Heat-induced conformational changes in proteins studied by electrospray ionization mass spectrometry, Anal. Chem. 65 (1993) 1–6.
[25] J.L.P. Benesch, F. Sobott, C.V. Robinson, Thermal dissociation of multimeric protein complexes by using nanoelectrospray mass spectrometry, Anal. Chem. 75 (2003) 2208–2214.
[26] H.J. Sterling, E.R. Williams, Origin of supercharging in electrospray ionization of noncovalent complexes from aqueous solution, J. Am. Soc. Mass Spectrom. 20 (2009) 1933–1943.
[27] G. Wang, R.R. Abzalimov, I.A. Kaltashov, Direct monitoring of heat-stressed biopolymers with temperature-controlled electrospray ionization mass spectrometry, Anal. Chem. 83 (2011) 2870–2876.
[28] X. Cong, Y. Liu, W. Liu, X. Liang, D.H. Russell, A. Laganowsky, Determining membrane protein-lipid binding thermodynamics using native mass spectrometry, J. Am. Chem. Soc. 138 (2016) 4346–4349.
[29] B. Hommersom, T. Porta, R.M.A. Heeren, Ion mobility spectrometry reveals intermediate states in temperature-resolved DNA unfolding, Int. J. Mass Spectrom. 14 (2017) 52–55.
[30] G. Li, S. Zheng, Y. Chen, Z. Hou, G. Huang, Reliable tracking in-solution protein unfolding via ultrafast thermal unfolding/ion mobility-mass spectrometry, Anal. Chem. 90 (2018) 7997–8001.
[31] D.R. Fuller, C.R. Conant, T.J. El-Baba, C.J. Brown, D.W. Woodall, D.H. Russell, D.E. Clemmer, Conformationally regulated peptide bond cleavage in bradykinin, J. Am. Chem. Soc. 140 (2018) 9357–9360.
[32] A. Marchand, F. Rosu, R. Zenobi, V. Gabelica, Thermal denaturation of DNA G-quadruplexes and their complexes with ligands: thermodynamic analysis of the multiple states revealed by mass spectrometry, J. Am. Chem. Soc. 140

(2018) 12553–12565.
[33] C.R. Conant, D.R. Fuller, T.J. El-Baba, Z. Zhang, D.H. Russell, D.E. Clemmer, Substance P in solution: trans-to-cis configurational changes of penultimate prolines initiate non-enzymatic peptide bond cleavages, J. Am. Soc. Mass Spectrom. 30 (2019) 919–931.
[34] D.E. Clemmer, R.R. Hudgins, M.F. Jarrold, Naked protein conformations: cytochrome c in the gas phase, J. Am. Chem. Soc. 117 (1995) 10141–10142.
[35] J.L.R. Arrondo, N.M. Young, H.H. Mantsch, The solution structure of concanavalin A probed by FT-IR spectroscopy, Biochim. Biophys. Acta 952 (1988) 261–268.
[36] K.D. Hardman, C.F. Ainsworth, Structure of concanavalin A at 2.4-Ang resolution, Biochemistry 11 (1972) 4910–4919.
[37] J.H. Naismith, C. Emmerich, J. Habash, S.J. Harrop, J.R. Helliwell, W.N. Hunter, J. Raftery, Kalb (Gilboa, A.J, J. Yariv, Refined structure of concanavalin A complexed with methyl [alpha]-D-mannopyranoside at 2.0 Å resolution and comparison with the saccharide-free structure, Acta Cryst D50 (1994) 847–858.
[38] J.W. Becker, G.N. Rekee, J.L. Wang, B.A. Cunningham, G.M. Edelman, The covalent and three-dimensional structure of concanavalin a III. Structure of the monomer and its interactions with metals and saccharides, J. Biol. Chem. 250 (1975) 1513–1524.
[39] G. Reeke, J.W. Becker, B.A. Cunningham, J.L. Wang, I. Yahara, G.M. Edelman, Structure and function of concanavalin A, Adv. Exp. Med. Biol. 55 (13) (1975) 13–33.
[40] T. Banerjee, N. Kishore, A differential scanning calorimetric study on the irreversible thermal unfolding of concanavalin A, Thermochim. Acta 411 (2004) 195–201.
[41] L. Han, B.T. Ruotolo, Hofmeister salts recover a misfolded multiprotein complex for subsequent structural measurements in the gas phase, Angew. Chem. Int. Ed. 52 (2013) 8329–8332.
[42] H. Hernandez, C.V. Robinson, Determining the stoichiometry and interactions of macromolecular assemblies from mass spectrometry, Nat. Protoc. 2 (2007) 715–726.
[43] B.T. Ruotolo, J.L.P. Benesch, A.M. Sandercock, S.J. Hyung, C.V. Robinson, Ion mobility-mass spectrometry analysis of large protein complexes, Nat. Protoc. 7 (2008) 1139–1152.
[44] M.F. Bush, Z. Hall, K. Giles, J. Hoyes, C.V. Robinson, B.T. Ruotolo, Collision cross sections of proteins and their complexes: a calibration framework and database for gas-phase structural biology, Anal. Chem. 82 (2010) 9557–9565.
[45] M.T. Marty, A.J. Baldwin, E.G. Marklund, G.K.A. Hochberg, J.L.P. Benesch, C.V. Robinson, Bayesian deconvolution of mass and ion mobility spectra: from binary interactions to polydisperse ensembles, Anal. Chem. 87 (2015) 4370–4376.
[46] S.E. Haynes, D.A. Polasky, S.M. Dixit, J.D. Majmudar, K. Neeson, B.T. Ruotolo, B.R. Martin, Variable-velocity traveling-wave ion mobility separation enhancing peak capacity for data-independent acquisition proteomics, Anal. Chem. 89 (2017) 5669–5672.
[47] V.J. LiCata, C.-C. Liu, Analysis of free energy versus temperature curves in protein folding and macromolecular interaction, Methods Enzymol. 488 (2011) 219–238.
[48] S. van der Walt, S.C. Colbert, G. Varoquaux, The NumPy array: a structure for efficient numerical computation, Comput. Sci. Eng. 13 (2011) 22–30.
[49] K.J. Millman, M. Aivazis, Python for scientists and engineers, Comput. Sci. Eng. 13 (2011) 9–12.
[50] J. D. Matplotlib Hunter, A 2D graphics environment, Comput. Sci. Eng. 9 (2007) 90–95.
[51] E.G. Marklund, M.T. Degiacoomi, C.V. Robinson, A.J. Baldwin, J.L.P. Benesch, Collisions cross sections for structural proteomics, Structure 23 (2015) 791–799.
[52] C. Bleiholder, S. Suhai, B. Paizs, Revising the proton affinity scale of the naturally occurring alpha-amino acids, J. Am. Soc. Mass Spectrom. 17 (2006) 1275–1281.
[53] A.R. Fersht, Structure and Mechanism in Protein Science, W. H. Freeman and Company, New York, NY, 2003, pp. 509–539.
[54] P.L. Privalov, G.I. Makhatadze, Contribution of hydration and non-covalent interactions to the heat capacity effect on protein unfolding, J. Mol. Biol. 224 (1992) 715–723.
[55] N.V. Prabhu, K. Sharp, Heat capacity in proteins, Annu. Rev. Phys. Chem. 56 (2005) 521–548.
[56] Y. Liu, J.M. Sturtevant, The observed change in heat capacity accompanying the thermal unfolding of proteins depends on the composition of the solution and on the method employed to change the temperature of unfolding, Biochemistry 35 (1996), 4059-3062.